IEEE Access
Multidisciplinary ⋮ Rapid Review ⋮ Open Access Journal

Received 13 June 2022, accepted 11 July 2022, date of publication 14 July 2022, date of current version 20 July 2022.

Digital Object Identifier 10.1109/ACCESS.2022.3190955

RESEARCH ARTICLE

Path Tracking Control With Four-Wheel Independent Steering, Driving and Braking Systems for Autonomous Electric Vehicles

YONGHWAN JEONG[1] AND SEONGJIN YIM[2], (Member, IEEE)
[1]Department of Mechanical and Automotive Engineering, Seoul National University of Science and Technology, Seoul 01811, Republic of Korea
[2]Research Center for Electrical and Information Technology, Seoul National University of Science and Technology, Seoul 01811, Republic of Korea

Corresponding author: Seongjin Yim (acebtif@seoultech.ac.kr)

This work was supported by the Ministry of Education through the National Research Foundation of Korea (NRF) under Basic Science Research Program (NRF-2019R1A6A1A03032119).

ABSTRACT This paper presents a method to design a path tracking controller with four-wheel independent braking (4WIB), drive (4WID) and steering (4WIS) systems equipped in in-wheel motor-driven electric vehicles (IWM-EVs). Generally, it is difficult to calculate the steering angles of 4WIS and the braking/traction torques of 4WIB/4WID for path tracking control. Moreover, there have been limitations of an error dynamics-based path tracking controller, which requires assumptions on a target path. To cope with these problems, the path tracking problem on a target path is converted into the yaw rate tracking one with a reference yaw rate in this paper. Two methods are adopted for the purpose of calculating a reference yaw rate. The first is to use a pure pursuit method, which generates a steering angle for path tracking. From the steering angle, a reference yaw rate is calculated. The second is to derive a reference yaw rate from a target path and a current vehicle position. For yaw rate tracking, direct yaw moment control is adopted to generate a control yaw moment. A control allocation method is adopted to distribute a control yaw moment into tire forces, generated by 4WIS, 4WID and 4WIB. Several actuator combinations are represented by various sets of virtual weights in the control allocation method. A simulation with a vehicle simulation program, CarSim®, shows that the proposed path tracking controller is effective in enhancing the path tracking performance with 4WIS, 4WID and 4WIB. From the simulation, effects of actuator combinations on path tracking performance are analyzed.

INDEX TERMS Path tracking control, Yaw rate tracking control, 4-wheel independent steering (4WIS), 4-wheel independent drive (4WID), 4-wheel independent braking (4WIB), in-wheel motor (IWM) system.

I. INTRODUCTION

The introduction of the active safety system has improved driving convenience and road safety by preventing accidents due to driver carelessness or unexpected external disturbances. The success of the active safety system led to the research on autonomous driving. Autonomous driving is expected as a solution for future transportation. Particularly, the road safety, traffic flow, and convenience of passengers can be improved by virtue of autonomous driving [1], [2].

In the earlier days, autonomous driving research was conducted on motorways, which have a relatively simple driving environment. To extend the operational design domain (ODD) of autonomous driving, various methodologies have been proposed and developed to cope with more complicated driving conditions [3]. Based on these studies, the ODD of autonomous driving has been expanded not only to highways, but also to parking lots, urban roads, and unstructured environments. These advances have required the development of both software and hardware for autonomous driving. In the case of software, various methods have been proposed to improve the perception, decision, and control. For hardware, the number of sensors and processors have

The associate editor coordinating the review of this manuscript and approving it for publication was Nasim Ullah.

been increased to acquire and process the more information. In addition, the number of actuators also increased to improve control performance and to achieve fault tolerant capability. As a result, the control allocation problem was formulated because an autonomous vehicle has multiple actuators for control purpose [4]. This problem should be solved to optimize control efforts needed for multiple actuators [5]–[12]. Recently, a purpose-built vehicle (PBV) began to adopt in-wheel motors (IWM), electro-mechanical brake (EMB) and 4-wheel independent steering (4WIS) modules to realize a flexible platform for various purpose of autonomous driving [13]–[18]. As a consequence, various researches have been conducted in the perspective of controller design for over-actuated vehicles.

To date, additional actuators have been introduced to improve the maneuverability and agility of a human driven vehicle. For example, electronic stability control (ESC), torque vectoring devices (TVD), 4-wheel drive (4WD), rear wheel steering (RWS) and 4-wheel steering (4WS) were introduced as an actuator for vehicle stability control [17]–[20]. Initially, an individual algorithm for a particular actuator were developed [21]–[24]. Recently, an integrated controller has been designed to achieve better performance by coordinating control efforts of multiple actuators.

Recent electrification changes the powertrain of a vehicle. In view of an actuator, E-corner module has been proposed as a future actuator for electric vehicles [25], [26]. Generally, the E-corner module consists of IWM, EMB, electric steering module, and active suspension. Therefore, the E-corner module has the four-wheel independent steering, driving, and braking functions (4WIS, 4WID, and 4WIB) [17]. Therefore, 4WIS, 4WID, and 4WIB can improve the control performance of not only a human-driven vehicle but also an autonomous vehicle.

Since current autonomous vehicles use an electric power steering (EPS), a path tracking controller has been designed for a front wheel steering (FWS) vehicle. Recent advances in path tracking control were summarized in the literature [27]–[32]. Among them, the path tracking control was investigated for a vehicle with 4WS or 4WD [4], [9], [16], [33]–[40]. The recent studies on the path tracking control with 4WS and 4WD are summarized in Table 1. In these researches, linear–quadratic regulator (LQR), H_∞ control, sliding mode control (SMC) and model predictive control (MPC) were adopted as a controller design methodology. As shown in Table 1, most of these researches have adopted the error dynamics based model for controller design. Because the path tracking problem is one of reference tracking one, various controllers have been designed to regulate path tracking errors. The lateral and heading errors were used to define the error dynamics. However, in this case, assumptions about the reference path are required. As a consequence, it is difficult to guarantee performance in various cases. For actuators, the 4WS system is considered as the integration of the FWS and RWS. In other words, the steering inputs of the left and right wheels were not calculated separately. Therefore, the effect of 4WIS on path tracking is not well discussed.

According to a careful review of the previous studies, 4WIS, 4WIB, and 4WID have been originally adopted for vehicle stability control [6], [17], [18], [41], [42]. On the contrary, there have been little studies on the path tracking control with a vehicle with 4WIS and/or 4WID [7], [10]–[12], [14], [15]. The recent studies on the path tracking control with 4WIS, 4WID and 4WIB are summarized in Table 1. With the view that 4WIS is an advanced system of 4WS, the steering angles of front and rear wheels were determined by 4WS based path tracking controller. Then, the control inputs were converted into steering angles of four wheels by a geometric relationship. However, it is difficult to fully utilize the advantages of 4WIS by simply distributing the steering angle to left and right by geometric relationships. Moreover, the error dynamics-based model were adopted in the other studies [7], [10], [15]. Therefore, the disadvantages of the error dynamics-based path tracking controller for the FWS or 4WS vehicles appear the same for 4WIS system.

Among the previous studies, a few papers did not adopt the error dynamics based model for path tracking controller design. The most notable feature of these papers is that the path tracking problem is converted into the yaw rate tracking one [11], [12], [14]. Similar to the chassis control methods, a reference yaw rate was derived from the steering angle of front wheels [11], [14]. In these papers, a driver model was adopted for steering angle generation. For example, the yaw angle tracking method was used to determine the front steering angle [14]. Since the reference yaw rate is derived from the front wheel steering model, it is difficult to use the possible yaw motion of 4WIS vehicles. To overcome this problem, a reference yaw rate was derived not from a driver model but from a target path [12]. For the reason, this research did not need a driver model.

In the previous study, the control inputs to 4WIS and 4WID were generated by separate controllers [14]. On the contrary, the other study determined the steering and driving torque of each wheel by adopting two-level control structure: upper- and lower-level controllers [11]. In the upper-level controller, a yaw moment is generated from PID and sliding mode controller. In the lower-level controller, the yaw moment is distributed into driving torques of 4WID and steering angles of 4WIS by considering the tire force under friction constraints. In addition, a optimization based control allocation method is proposed to distribute the yaw moment to four wheels [4], [17]–[20]. Another study adopted MPC to generate driving torques of 4WID and steering angles of 4WIS for yaw rate tracking. Different from the previous study [11], MPC can directly determine the driving torques and the steering angles without the upper- and lower-level controllers [12]. However, MPC requires a large amount of computation time in real application.

The problem formulation of this paper is summarized as the following paragraph. This paper follows the idea that the path tracking problem is converted into yaw rate tracking one

TABLE 1. Survey on recent studies for path tracking control with 4WS, 4WD, 4WIS, 4WID and 4WIB.

Model	Controller	Actuator	Simulation/Experiment	Reference
Bicycle model + Error dynamics model	SMC	4WS	Simulation	[5]
Planar model + Error dynamics model	DOB-based control	4WIS/4WID	Simulation	[7]
Bicycle model + Error dynamics model	LPV/H_∞ controller	4WS	Simulation	[9]
Bicycle model + Error dynamics model	LQR	4WIS/4WID	Simulation/Experiment	[10]
Planar model	MPC	4WIS/4WID/4WIB	Simulation	[12]
Bicycle model + PID driver model	LQR for 4WIS, SMC for 4WID	4WIS/4WID	Simulation	[14]
Bicycle model + Error dynamics model	MPC	4WIS/4WID	Simulation	[15]
Bicycle model + Error dynamics model	LQR + Feedforward control	4WS	Experiment	[16]
Bicycle model + Error dynamics model	State feedback control	4WS	Simulation	[33]
Bicycle model + Error dynamics model	SMC + Feedforward control	4WS	Simulation	[34]
Bicycle model + Error dynamics model	Robust adaptive SMC	4WS	Simulation	[35]
Bicycle model + Error dynamics model	SMC	4WS	Simulation	[36]
Bicycle model + Error dynamics model	MPC	4WS	Simulation	[37]
Planar model + Error dynamics model	MPC+SQP, PSO-based method	4WS/4WD	Simulation	[38]
Bicycle model + Error dynamics model	MPC for FWS, LQR for 4WS	4WS	Simulation/Experiment	[39]
Bicycle model + Error dynamics model	Optimal predictive control	4WS	Simulation	[40]
Planar model + Error dynamics model	PID, SMC	4WIS/4WID	Simulation	[41]

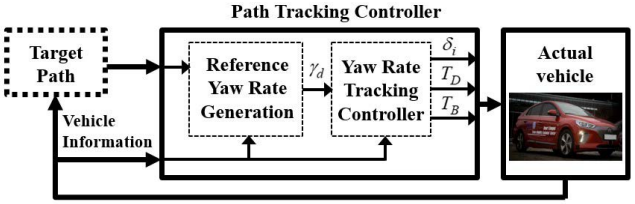

FIGURE 1. Schematic diagram of the path tracking controller.

and that a controller has two-level structure [11]. Fig. 1 shows the schematic diagram of the path tracking controller proposed in this paper. As shown in Fig. 1, the reference yaw rate is generated in Reference Yaw Rate Generation module. In the module, the reference yaw rate is generated from two sources. The first is the steering angle of front wheels generated by a driver model [11]. The second is a target path [12]. A vehicle has 4WIS, 4WID and 4WIB functions. Yaw Rate Tracking Controller in Fig. 1 has two-level structure: the upper- and lower-level controllers. For yaw rate tracking with the vehicle, a direct yaw moment controller is designed in the upper-level controller. This controller generates a control yaw moment needed to make a vehicle follow the reference yaw rate. In the lower-level controller, a control allocation scheme is adopted to distribute the control yaw moment into tire forces generated by the actuators [4]. Weighted pseudo-inverse based control allocation (WPCA) was adopted as the control allocation method. WPCA is an equality-constrained quadratic programming, which can be algebraically solved in real-time [17]–[20]. The optimum tire forces obtained by WPCA are converted into the driving/braking torques of 4WID and 4WIB, and into the steering angles of 4WIS, respectively. Generally, 4WID and 4WIB have been developed and studied for vehicle stability control. In other words, these actuators are needed on low-friction roads, where a vehicle can easily lose its lateral stability. However, 4WID and 4WIB have little effects on the control performance for vehicle stability according to the previous study [17]. For the reason, the effects of 4WID and 4WIB are checked on the path tracking performance.

The key contributions in this work are summarized as follows:

1. To solve the path tracking problem for a vehicle with 4WIS, 4WID and 4WIB, it is converted to the yaw tracking one. Then, the yaw rate tracking controller which has two-level control structure is designed.

2. The reference yaw rate is generated from two sources. The first is the steering angles of front wheels generated by a driver model. The second is a target path. These methods do not require assumptions on the road shapes and vehicle models. The path tracking performance of these two methods is compared with each other.

3. Difference from the MPC proposed in the previous work, WPCA is adopted for yaw moment distribution in this paper. WPCA is relevant to real-time applications because it can algebraically solve the quadratic programming.

This paper is organized as follows: Section II describes how to generate a reference yaw rate from a driver model or a target path. In Section III, the yaw rate tracing controller is designed and control allocation method is introduced. The proposed method is evaluated on vehicle simulation software, CarSim, and is compared with conventional approaches in Section IV. Section V provides conclusions and future works regarding the proposed method.

II. DERIVATION OF REFERENCE YAW RATE

A path tracking controller has been designed with lateral offset and heading errors between a target path and vehicle position [25]–[30]. For path tracking control, a driver model has been commonly used on a FWS vehicle [27], [31]. A driver model is a controller which tries to make the errors zero. A driver model calculates the steering angle of front wheels.

Typical driver model for path tracking control is pure pursuit and Stanley methods. Another method is to use an error dynamics on a target path and to apply optimal control

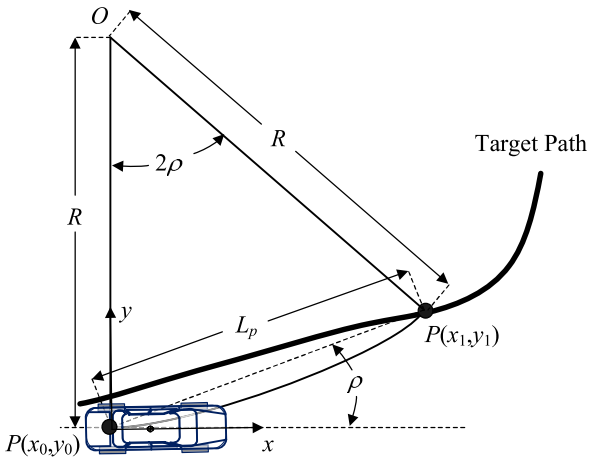

FIGURE 2. The geometry of pure pursuit method.

methodologies or sliding mode control with it for controller design [33]–[40]. In the method, the errors of the lateral offset and heading are used to define the plant model for controller design. However, it is difficult to correlate the lateral behavior of a vehicle to those errors because those have a different dimension from the lateral motion described by yaw rate and lateral acceleration. Moreover, an assumption on road geometry is required to derive the error dynamics. The state vector of the error dynamics consists of the lateral offset and heading errors. This means that a road shape should be defined as a differentiable function when obtaining the derivative of those errors. Therefore, there is a possibility that the path tracking performance may not be achieved in several driving situations where assumptions on road shapes cannot be held. To overcome these limitations of the path tracking controllers designed with error dynamics, a controller which does not need the error dynamics was proposed in the previous study [11], [12]. This paper adopts the idea of the paper.

A. PURE PURSUIT METHOD FOR STEERING ANGLE GENERATION

In this paper, a pure pursuit method is adopted as a driver model. Fig. 2 shows the geometry for pure pursuit method [32]. In Fig. 2, $P(x_0, y_0)$ and $P(x_1, y_1)$ are the points located on the center of rear axle and the target point on the target path, respectively. ρ is the angle between the vehicle's heading vector and the look-ahead one, which is called heading error. L_p and R are the look-ahead distance and the radius of the circular arc, respectively. In the pure pursuit method, the steering angle is determined only with L_p and ρ. From Fig. 2, the curvature κ of the circular arc connecting $P(x_0, y_0)$ and $P(x_1, y_1)$ is calculated as (1). With the definition of κ, the front steering angle is calculated as (2) [32]. In (2), L is the wheelbase, i.e., the distance between the front and rear axles.

$$\kappa = \frac{2\sin\rho}{L_p} \tag{1}$$

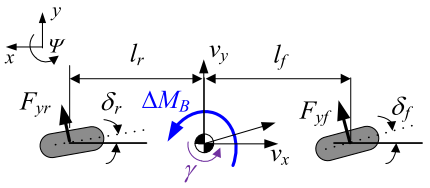

FIGURE 3. 2-DOF bicycle model.

$$\delta_f = \tan^{-1}(\kappa L) = \tan^{-1}\left(\frac{2L\sin\rho}{L_p}\right) \tag{2}$$

As shown in (2), the pure pursuit method generates the steering angle of a vehicle with FWS, which is the most common case. However, it is difficult for one to derive the steering angles of 4WIS from (2) with the pure pursuit method. This fact is common to the other driver models such as Stanley method and PID control [31]. The error dynamics based path tracking controller can be used for a vehicle with 4WS because the front and rear steering angles are explicitly expressed as a control input of the controllers such as LQR and MPC [33]–[40]. However, in this case, assumptions on a target path are required to build the error dynamics. Therefore, it is difficult to guarantee the path tracking performance on various road conditions. On the other hand, 4WS and 4WIS were adopted as a steering actuator for yaw rate tracking controller in the previous studies [17], [18]. In other words, 4WS and 4WIS can be easily handled from the viewpoint of yaw rate tracking control. For the reason, the path tracking control is converted into the yaw rate tracking one in this paper. When using the yaw rate tracking controller, it is necessary to derive the reference yaw rate from the front steering angle.

B. DERIVATION OF REFERENCE YAW RATE FROM A BICYCLE MODEL

The most commonly adopted method to generate the reference yaw rate from the steering angle is to use the steady-state motion of a bicycle model. Fig. 3 shows the free-body diagram of 2-DOF bicycle model [17]–[20], [43], [44]. This model describes the motions of yaw and lateral directions under the assumption that the longitudinal velocity v_x is constant. Hence, there are two state variables in the model: the yaw rate, γ, and the lateral velocity, v_y. With the state variables, the equations of motions for this model are derived as (3) [43], [44]. Tire slip angles of the front and rear wheels, α_f and α_r, are calculated as (4) using γ, v_y, and v_x. In (3), the lateral tire forces of the front and rear wheels, F_{yf} and F_{yr}, are assumed to be proportional to the tire slip angles, α_f and α_r, as given in (5), respectively. The reference yaw rate, γ_d, is derived as (6) using the steering angle of front wheels, δ_f, and the longitudinal velocity, v_x, from steady-state relation between steering angle and radius of vehicle trajectory [44]. As shown in (6), the reference yaw rate is directly calculated from the front steering angle. This means that the reference yaw rate can be easily calculated from the front steering

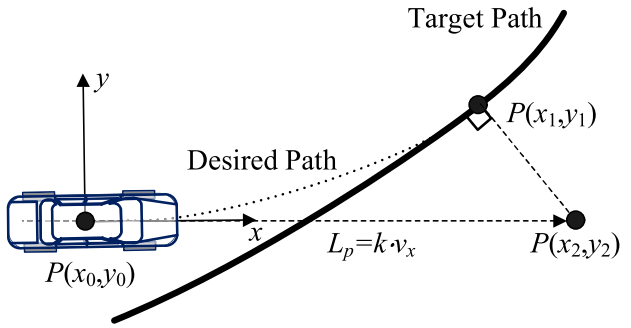

FIGURE 4. Geometry of the desired and target paths with the preview point.

angle regardless of a driver model used for steering angle generation. The steering angle of front wheels is generated by the pure pursuit method. Let the reference yaw rate derived from the pure pursuit method as PPM-RYR.

$$\begin{cases} m\left(\dot{v}_y + \gamma v_x\right) = F_{yf}\cos\delta_f + F_{yr}\cos\delta_r \\ I_z\dot{\gamma} = l_f F_{yf}\cos\delta_f - l_r F_{yr}\cos\delta_r + \Delta M_B \end{cases} \tag{3}$$

$$\alpha_f = \delta_f - \frac{v_y + l_f\gamma}{v_x} \alpha_r = \delta_r - \frac{v_y - l_r\gamma}{v_x} \tag{4}$$

$$F_{yf} = -2C_f\alpha_f, F_{yr} = -2C_r\alpha_r \tag{5}$$

$$\gamma_d = \frac{C_f \cdot C_r \cdot \left(l_f + l_r\right) \cdot v_x}{C_f \cdot C_r \cdot \left(l_f + l_r\right)^2 + m \cdot v_x^2 \cdot \left(l_r \cdot C_r - l_f \cdot C_f\right)} \cdot \delta_f \tag{6}$$

C. DERIVATION OF REFERENCE YAW RATE FROM TARGET PATH

The reference yaw rate can be derived from a target path without a bicycle model or error dynamics [12]. Fig. 4 shows the desired and target paths with the preview point. In Fig. 4, the target path is marked as a black line. The desired path, marked as a dotted line in Fig. 4, is defined by connecting the center of gravity (C.G.) of the vehicle, $P(x_0, y_0)$, with the preview point on the target path, $P(x_1, y_1)$. To get the point, $P(x_1, y_1)$, a preview distance L_p is determined by the formula, $k \cdot v_x$, where k is the proportional gain. The value of the proportional gain k is set to 1.2. The desired path is used to determine the reference yaw rate, which means the yaw rate needed to move the vehicle to the preview point.

Under the assumption that a side-slip angle of the vehicle is small and, then, negligible, the reference yaw rate can be calculated from the curvature κ_d of the desired path. Because the point $P(x_1, y_1)$ is not far from the vehicle, the desired path can be modeled as a 2nd-order polynomial as given in (7). To determine the coefficients of (7), three constraints are needed because it has three unknowns. For position constraints, the coordinates of two points, $P(x_0, y_0)$ and $P(x_1, y_1)$, are used. The slope at $P(x_0, y_0)$ is used as the heading constraint. With the information, three constraints are obtained as (8). Thus, the coefficients of (7) are obtained by solving (8). With the desired path (7) determined by (8), the curvature κ_d at the point $P(x_0, y_0)$ is calculated as (9). Finally, the reference yaw rate γ_d for path tracking is calculated as (10) [12]. Let the reference yaw rate derived from a target path as PATH-RYR.

$$y(x) = ax^2 + bx + c \tag{7}$$

$$\begin{bmatrix} y_0 \\ y_1 \\ y'(x_0) \end{bmatrix} = \begin{bmatrix} x_0^2 & x_0 & 1 \\ x_1^2 & x_1 & 1 \\ 2x_0 & 1 & 0 \end{bmatrix} \begin{bmatrix} a \\ b \\ c \end{bmatrix} \tag{8}$$

$$\kappa_d = \frac{y''(x_0)}{\left\{1 + y'(x_0)^2\right\}^{3/2}} = \frac{2a}{\left\{1 + (2ax_0 + b)^2\right\}^{3/2}} \tag{9}$$

$$\gamma_d = v_x \cdot \kappa_d \tag{10}$$

III. DESIGN OF YAW RATE TRACKING CONTROLLER

A. DESIGN OF REFERENCE TRACKING CONTROLLER

To make a vehicle follow the reference yaw rate γ_d for path tracking, a direct yaw moment control has been adopted with 2-DOF bicycle model, as given in Fig. 3 [17]–[20]. In this paper, the direct yaw moment control is adopted for yaw rate tracking.

The basic objective of the yaw rate tracking controller is to make a vehicle follow the reference yaw rate. In other words, the difference or error between the reference yaw rate and real one should be minimized or zero. Another objective is to minimize the side-slip angle, β, defined in (11). β should be maintained less than 3° for lateral stability, especially on slippery roads [18], [43], [44]. The error surface is defined as (12). In (12), η is the parameter used to tune the trade-off between the yaw rate tracking and the lateral stability. The value of η is set to 1 for all simulation cases. The convergence condition for the error surface is given as (13). This condition should be satisfied to make the error surface zero [17]–[20], [44]. From (12), (13) and (3), the control yaw moment ΔM_B is obtained as (14). In (11), the lateral velocity v_y is estimated with the estimator presented in the previous study [45]. In (14), it is difficult or too expensive to measure F_{yf} and F_{yr} with a sensor. Thus, F_{yf} and F_{yr} are estimated by a sliding mode observer, as given in [46].

$$\beta = \tan^{-1}\left(\frac{v_y}{v_x}\right) \tag{11}$$

$$e_\gamma = (\gamma - \gamma_d) + \eta\beta \tag{12}$$

$$\dot{e}_\gamma = -K_\gamma e_\gamma \left(K_\gamma > 0\right) \tag{13}$$

$$\begin{aligned} \Delta M_B = {} & I_z \cdot \dot{\gamma}_d \\ & + I_z \cdot \eta \cdot \left(\frac{F_{yf}\cos\delta_f + F_{yr}\cos\delta_r}{mv_x} - \gamma\right) \\ & - l_f F_{yf}\cos\delta_f + l_r F_{yr}\cos\delta_r - I_z \cdot K \cdot e_\gamma \end{aligned} \tag{14}$$

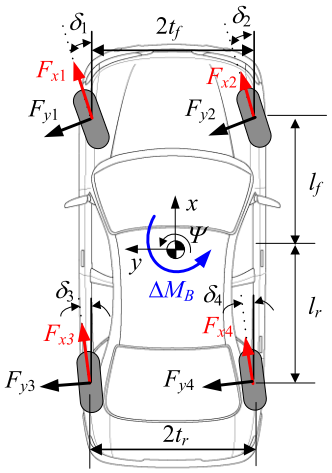

FIGURE 5. Coordinate system corresponding to tire forces and control yaw moment.

B. CONTROL ALLOCATION FROM THE CONTROL YAW MOMENT TO TIRE FORCES

Subsequent to computation of ΔM_B from the direct yaw moment control, it should be distributed into tire forces, generated by actuators, with a control allocation algorithm. Fig. 5 shows ΔM_B and the tire forces at four wheels in a vehicle. In Fig. 5, the wheel indices 1,2,3, and 4 represent the front left, front right, rear left and rear right wheels, respectively. In Fig. 5, the lateral tire forces, F_{y1}, F_{y2}, F_{y3}, and F_{y4}, are generated by 4WIS, and the longitudinal tire forces, F_{x1}, F_{x2}, F_{x3} and F_{x4}, representing braking or traction one, are generated by 4WID or 4WIB.

In this paper, it is assumed that there are three steering actuators: FWS, 4WS and 4WIS. In Fig. 5, the steering angles, δ_1, δ_2, δ_3, and δ_4, generated by a steering actuator can be set for FWS, 4WS and 4WIS. In this case, FWS and 4WS are the subfunctions of 4WIS. For example, the steering angles are set to $\delta_1 = \delta_2, \delta_3 = \delta_4 = 0$ if FWS is adopted as a steering actuator. From the fact, the steering angles are set as (15) for each steering actuator. These steering angles are calculated from the lateral tire forces, F_{y1}, F_{y2}, F_{y3} and F_{y4}.

$$\begin{aligned} &\text{FWS}: \ \delta_1 = \delta_2 \ \ (\delta_3 = \delta_4 = 0) \\ &\text{4WS}: \ \delta_1 = \delta_2, \ \delta_3 = \delta_4 \\ &\text{4WIS}: \delta_1, \ \delta_2, \ \delta_3, \ \delta_4 \end{aligned} \tag{15}$$

From Fig. 4, the geometric relationship between the tire forces and ΔM_B is derived as (16) from force-moment equilibrium. The elements of the vector $\mathbf{g}$ in (16) are derived as (17) from Fig. 5. In Fig. 5, the tire forces should be determined such that (16) is satisfied. This is called the control allocation problem [4]. The control allocation of ΔM_B into tire forces is called the yaw moment distribution [17]–[20]. For yaw moment distribution, the WPCA is adopted in this paper [18]–[20], [45], [46].

$$\underbrace{\begin{bmatrix} a_1 & a_2 & a_3 & a_4 & a_5 & a_6 & a_7 & a_8 \end{bmatrix}}_{\mathbf{g}} \underbrace{\begin{bmatrix} F_{y1} \\ F_{y2} \\ F_{y3} \\ F_{y4} \\ F_{x1} \\ F_{x2} \\ F_{x3} \\ F_{x4} \end{bmatrix}}_{\mathbf{x}} = \Delta M_B \tag{16}$$

$$\begin{aligned} a_1 &= -l_f \cos\delta_1 - t_f \sin\delta_1, a_2 = -l_f \cos\delta_2 + t_f \sin\delta_2, \\ a_3 &= l_r \cos\delta_3 - t_r \sin\delta_3, a_4 = l_r \cos\delta_4 + t_r \sin\delta_4, \\ a_5 &= -l_f \sin\delta_1 + t_f \cos\delta_1, a_6 = -l_f \sin\delta_2 - t_f \cos\delta_2, \\ a_7 &= l_r \sin\delta_3 + t_r \cos\delta_3, a_8 = l_r \sin\delta_4 - t_r \cos\delta_4 \end{aligned} \tag{17}$$

There are no constraints on the lateral forces in (16), which means that the steering angles, δ_1, δ_2, δ_3, and δ_4, can be freely generated by 4WIS. However, this cannot represent the constrains on the steering angles imposed by FWS and 4WS, as given in (15). The conditions of (15) representing FWS and 4WS can be represented by the equality constraints, (18) and (19), with the vector $\mathbf{x}$, respectively [18]. By incorporating (18) and (19) into (16), new equality constraints for FWS and 4WS are obtained as (20) and (21), respectively.

$$\begin{bmatrix} 1 & -1 & 0 & 0 & 0 & 0 & 0 & 0 \end{bmatrix} \mathbf{x} = 0 \tag{18}$$

$$\begin{bmatrix} 1 & -1 & 0 & 0 & 0 & 0 & 0 & 0 \\ 0 & 0 & 1 & -1 & 0 & 0 & 0 & 0 \end{bmatrix} \mathbf{x} = \begin{bmatrix} 0 \\ 0 \end{bmatrix} \tag{19}$$

$$\underbrace{\begin{bmatrix} \mathbf{g} \\ 1 & -1 & 0 & 0 & 0 & 0 & 0 & 0 \end{bmatrix}}_{\mathbf{H}} \mathbf{x} = \underbrace{\begin{bmatrix} \Delta M_B \\ 0 \end{bmatrix}}_{\mathbf{M}} \tag{20}$$

$$\underbrace{\begin{bmatrix} g \\ 1 & -1 & 0 & 0 & 0 & 0 & 0 & 0 \\ 0 & 0 & 1 & -1 & 0 & 0 & 0 & 0 \end{bmatrix}}_{\mathbf{H}} \mathbf{x} = \underbrace{\begin{bmatrix} \Delta M_B \\ 0 \\ 0 \end{bmatrix}}_{\mathbf{M}} \tag{21}$$

To determine the tire forces in Fig. 5, an optimization problem is formulated. The quadratic objective function is defined as (22). In (22), the term, μF_{zi}, product of the tire-road friction coefficient μ and the vertical tire force F_{zi}, stands for the radius of friction circle at each wheel [48]. This value cannot be measured. So, it should be estimated. The vertical tire force F_{zi} can be estimated from the longitudinal and lateral acceleration signals. In (22), ρ is the vector of virtual weights ρ_i, as defined in (23). The optimization problem, as given in (16) and (22), is a quadratic programming problem with a single equality constraint. By applying the method of Lagrange multiplier to the problem, the optimum solution is easily calculated as (24). This is called weighted pseudo-inverse based control allocation (WPCA) [17]–[20],

[47], [48].

$$\begin{cases} J = \frac{\rho_1 F_{y1}^2 + \rho_5 F_{x1}^2}{\mu F_{z1}^2} + \frac{\rho_2 F_{y2}^2 + \rho_6 F_{x2}^2}{\mu F_{z2}^2} \\ + \frac{\rho_3 F_{y3}^2 + \rho_7 F_{x3}^2}{\mu F_{z3}^2} + \frac{\rho_4 F_{y4}^2 + \rho_8 F_{x4}^2}{\mu F_{z4}^2} = \mathbf{x}^T \mathbf{W} \mathbf{x} \\ \mathbf{v} = \left[\frac{1}{\mu F_{z1}^2} \ \frac{1}{\mu F_{z2}^2} \ \frac{1}{\mu F_{z3}^2} \ \frac{1}{\mu F_{z4}^2} \right] \\ \mathbf{W} = \mathrm{diag}\left[\mathbf{v} \ \mathbf{v} \right] \rho \end{cases} \tag{22}$$

$$\rho = \left[\rho_1 \ \rho_2 \ \rho_3 \ \rho_4 \ \rho_5 \ \rho_6 \ \rho_7 \ \rho_8 \right]^T \tag{23}$$

$$\mathbf{x}_{opt} = \begin{cases} \mathbf{W}^{-1}\mathbf{g}^T \left(\mathbf{g}\mathbf{W}^{-1}\mathbf{g}^T \right)^{-1} \Delta M_B, \text{4WIS} \\ \mathbf{W}^{-1}\mathbf{H}^T \left(\mathbf{H}\mathbf{W}^{-1}\mathbf{H}^T \right)^{-1} \mathbf{M}, \ \text{FWS, 4WS} \end{cases} \tag{24}$$

The vector of virtual weights, ρ, has been used to represent several actuator combinations. For example, one of the steering actuators, FWS, 4WS and 4WIS can be combined with one of 4WID, 4WIB, and 4WID+4WIB [17]–[20]. The first four elements in ρ represent the availability of 4WIS, and the last four elements in ρ do the availability of 4WID and 4WIB at each wheel. It is assumed that ε is a very small value, i.e., 1e-4. The steering actuators, FWS, 4WS and 4WIS, are represented with the ρ given in (25). Under the first condition of (25), only the lateral tire forces, F_{y1} and F_{y2}, are generated as non-zero values from the optimization, and the other lateral tire forces are obtained as zero. The vectors of virtual weights representing the actuator combinations, 4WID, 4WIB and 4WIS+4WIB, are given in (26), (27) and (28), respectively. If 4WIS, 4WID and 4WIB are available, then all the virtual weights in ρ are set to a particular non-zero identical value. The detailed explanation on how to represent several actuator combinations with ρ can be found in the previous studies [17]–[20].

$$\begin{cases} \boldsymbol{\rho} = \left[\varepsilon \ \varepsilon \ 1 \ 1 \bullet \bullet \bullet \bullet \right]^T, \ \text{FWS} \\ \boldsymbol{\rho} = \left[\varepsilon \ \varepsilon \ \varepsilon \ \varepsilon \bullet \bullet \bullet \bullet \right]^T, \ \text{4WS,4WIS} \end{cases} \tag{25}$$

$$\begin{cases} \boldsymbol{\rho} = \left[\bullet \bullet \bullet \bullet \ 1 \ \varepsilon \ 1 \ \varepsilon \right]^T, \ \Delta M_B > 0 \\ \boldsymbol{\rho} = \left[\bullet \bullet \bullet \bullet \ \varepsilon \ 1 \ \varepsilon \ 1 \right]^T, \ \Delta M_B < 0 \end{cases} \tag{26}$$

$$\begin{cases} \boldsymbol{\rho} = \left[\bullet \bullet \bullet \bullet \ \varepsilon \ 1 \ \varepsilon \ 1 \right]^T, \ \Delta M_B > 0 \\ \boldsymbol{\rho} = \left[\bullet \bullet \bullet \bullet \ 1 \ \varepsilon \ 1 \ \varepsilon \right]^T, \ \Delta M_B < 0 \end{cases} \tag{27}$$

$$\begin{cases} \boldsymbol{\rho} = \left[\bullet \bullet \bullet \bullet \ \varepsilon \ \varepsilon \ \varepsilon \ \varepsilon \right]^T, \ \Delta M_B > 0 \\ \boldsymbol{\rho} = \left[\bullet \bullet \bullet \bullet \ \varepsilon \ \varepsilon \ \varepsilon \ \varepsilon \right]^T, \ \Delta M_B < 0 \end{cases} \tag{28}$$

As mentioned earlier, the target vehicle is equipped with an IWM system. Generally, 4WID is natural in the IWM system because an electric motor in a wheel can be driven independently. In this paper, it is assumed that an electro-mechanical braking (EMB) system is equipped with the IWM system. If EMB is available on each IWM system, the vehicle has 4WIB function. It is also assumed that regenerative braking is not used or activated for braking in this paper.

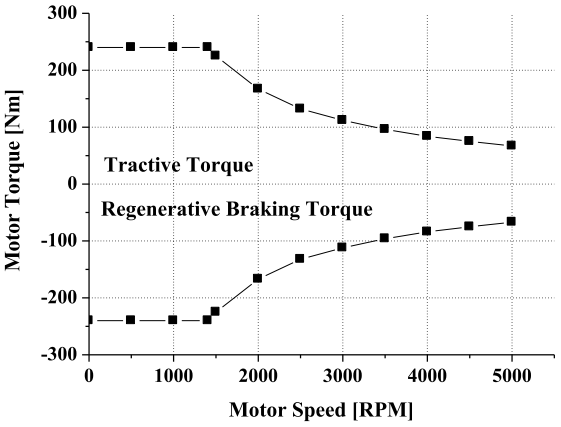

FIGURE 6. Characteristic curve of motor in IWM system.

After obtaining the solution of the optimization, $\mathbf{x}_{opt}$, the longitudinal tire force, F_{xi}, of the wheel i are converted into the traction torque, T_{Di}, as given in (29) if F_{xi} is positive. In (29), r_{wi} is the radius of the wheel i, and ω_i and g are the rotational speed and reduction gear ratio of an electric motor in IWM. In (29), $h(\bullet)$ represents the constraint imposed by a capacity curve of an electric motor in IWM. Fig. 6 shows the capacity curve of the electric motor used for an electric vehicle with independent rear-wheel drive [49]. If F_{xi} is negative, the braking torque, T_{Bi}, is calculated with (30), and directly applied to the wheel i. The braking torque can be generated by an EMB in IWM system. The method how to decide the steering angles of 4WIS will be given in the next subsection.

$$T_{Di} = \begin{cases} h\left(\frac{r_{wi} F_{xi}}{g}, \omega_i \right) & \text{if } F_{xi} > 0 \\ 0 & \text{if } F_{xi} \leq 0 \end{cases} \tag{29}$$

$$T_{Bi} = \begin{cases} r_{wi} \left| F_{xi} \right| & \text{if } F_{xi} > 0 \\ 0 & \text{if } F_{xi} \leq 0 \end{cases} \tag{30}$$

C. HOW TO DETERMINE STEERING ANGLES OF 4WS AND 4WIS FROM TIRE FORCES

After obtaining the lateral tire forces, $F_{y1\sim4}$, from the optimization problem, these should be converted into appropriate steering angles of FWS, 4WS and 4WIS. In the previous study, five methods were proposed for the purpose [18]. In this paper, two methods are adopted among them.

The simplest method is to use a linearized model of F_{yf} and F_{yr}, as shown in (5). From (5), δ_i can be obtained as (31) by regarding the slip angle as the steering one [17], [18]. In (31), F_{yi} and α_i are regarded as a linear relation and nonlinearity between them is neglected. In (31), C_i is the cornering stiffness of each wheel, and σ is the parameter used to tune the magnitude of C_i. In fact, σ can be regarded as a slip ratio between tire and road surface [42]. In general, reducing σ can enhance cornering performance because it generates larger δ_i. Let denote this method as Method#1.

TABLE 2. Parameters of F-class sedan in CarSim.

m_s	1,823kg	l_f	1.265m
I_z	6,286kg-m2	l_r	1.900m
C_f	62,000N/rad	t_f	0.80m
C_r	44,000N/rad	t_r	0.80m

Another method is to use the definition of the slip angle, as given in (4) [12], [17], [18], [42]–[44]. Equation (4) is derived from the bicycle model. So, it can be applied not to 4WIS but to FWS and 4WS. From (4) and (31), the steering angles of FWS and 4WS are calculated as (32) [42]. On the other hand, 4WIS has distinct slip angles for four wheels. Hence, (32) is cannot be used for 4WIS. For the vehicle with four wheels as given in Fig. 5, the slip angles of each wheel are calculated with (33). From (31) and (33), the steering angles of 4WIS are easily calculated as (34). For (32) and (34), the lateral velocity v_y is estimated with the estimator presented in the previous study [50]. Let denote this method as Method#2. In this paper, these two methods, Method#1 and Method#2, are compared with each other.

$$\alpha_i = -\frac{F_{yi}}{\sigma C_i}, i = 1, 2, 3, 4 \tag{31}$$

$$\delta_f = -\frac{F_{yf}}{\sigma C_f} + \frac{v_y + l_f\gamma}{v_x}, \delta_r = -\frac{F_{yr}}{\sigma C_r} + \frac{v_y - l_r\gamma}{v_x} \tag{32}$$

$$\begin{cases} \alpha_i = \delta_i - \frac{v_y + l_f\gamma}{v_x + (-1)^i t_f\gamma}, i = 1, 2 \\ \alpha_i = \delta_i - \frac{v_y - l_r\gamma}{v_x + (-1)^i t_r\gamma}, i = 3, 4 \end{cases} \tag{33}$$

$$\begin{cases} \delta_i = -\frac{F_{yi}}{\sigma C_i} + \frac{v_y + l_f\gamma}{v_x + (-1)^i t_f\gamma}, i = 1, 2 \\ \delta_i = -\frac{F_{yi}}{\sigma C_i} + \frac{v_y - l_r\gamma}{v_x + (-1)^i t_r\gamma}, i = 3, 4 \end{cases} \tag{34}$$

IV. VALIDATION WITH SIMULATION

In this section, simulation study has been done to verify the performance of the path tracking controller for a vehicle with 4WIS, 4WIB and 4WID. Because 4WIS can play a role as FWS and 4WS, three steering actuators, FWS, 4WS and 4WIS, are adopted for the yaw rate tracking controller.

The path tracking controller was implemented on MATLAB/Simulink and CarSim [50]. As described in the previous studies, the double lane change maneuver on moose test track at high speed is so severe that any other maneuvers can be covered by it [17]–[19]. Hence, this was adopted in the simulation. The initial vehicle speed was set to 50 km/h and maintained as constant using a speed controller of CarSim. Tire-road friction coefficient, μ, was set to a constant value, 0.85, which stands for normal asphalt surface.

For the simulation, a F-segment sedan model was chosen, which is a built-in model in CarSim. The parameters of F-segment sedan are shown in Table 2. The actuators, 4WIS, 4WID and 4WIB, were modelled as the 1st-order system. Time constants of these systems were set to 0.1. In 4WID, the capacity curve and the maximum power of the electric motor and the reduction gear ratio in IWM were cited from the previous study [49].

For comparison, the pure pursuit method was adopted as a base controller. Two path tracking controllers, i.e., yaw rate tracking controllers with PPM-RYR and PATH-RYR, are compared with each another.

Two set of simulaitons were done for the purpose of verifying the performance of the proposed path tracking controller. The first set is conducted for comparison between the proposed controller with the base controller. The second set is conducted to verify the performance of several actuator combinations such as 4WIS, 4WIS+4WID, 4WIS+4WIB and 4WIS+4WID+4WIB in the path tracking controller.

A. PERFORMANCE OF THE PATH TRACKING CONTROLLER

The first simulation has been conducted to verify the performance of the proposed path tracking controller. Three steering actuators, FWS, 4WS and 4WIS, are compared with one another. PPM-RYR is used as a reference yaw rate. For steering angle determination from the optimal lateral tire forces, Method#2 was adopted. Figs. 7 and 8 show the simulation results and the steering angles for three steering actuators. In those figures, the legend PPM represents the pure pursuit method used without yaw rate tracking controller. In Fig. 8, the legends FL, FR, RL and RR represents the front left, front right, rear left and rear right wheels, respectively. In the simulation results, the speed variation from the initial speed was less than 1km/h. So, it was not presented in the simulation results.

As shown in Fig. 7-(a), -(b), -(e) and -(f), the steering wheel angles, yaw rates, trajectories and lateral offset errors of FWS, 4WS and 4WIS with PPM-RYR are nearly identical to one another. As shown in Fig.7-(d), 4WS gives the smallest value of the maximum absolute value of the side-slip angle, compared to those of each actuator. This is the feature of 4WIS presented in the previous studies [17]–[19]. However, the yaw rate error of 4WIS is smaller than those of 4WS and 4WS, as shown in Fig. 7-(c). Nevertheless, the lateral offset errors of FWS, 4WS and 4WIS are smaller than that of the pure pursuit method. This means that the path tracking performance of the yaw rate tracking controller with FWS, 4WS and 4WIS is better than the pure pursuit method. As shown in Fig. 8, the steering angles of FWS, 4WS and 4WIS are nearly the same as the pure pursuit method because those are run on the identical target path. As a consequence, FWS, 4WS and 4WIS are recommended as a steering actuator for the yaw rate tracking controller. Among them, 4WS is recommended for ride comfort because it can give the smallest side-slip angle.

The simulation was done to check the effects of the methods of the reference yaw rate generation and the steering angle determination on the control performances. With FWS, 4WS and 4WIS, the simulation was done for four cases corresponding to the combinations of PPM-RYR and PATH-RYR with Method#1 and Method#2.

Fig. 9 shows the maximum absolute values of each measure for four cases. PPM-RYR.M1 in the tick labels of x-axis in

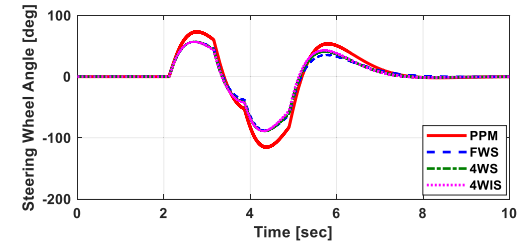

(a) Steering wheel angle of the pure pursuit method

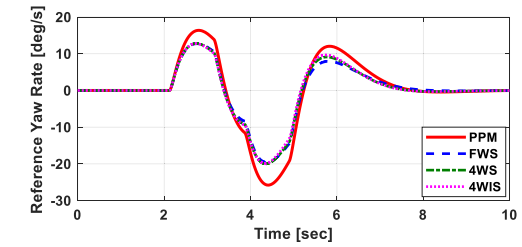

(b) Yaw rates from the pure pursuit method

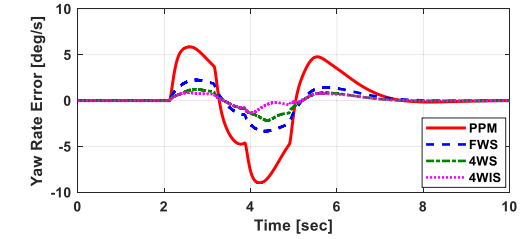

(c) Yaw rate erros

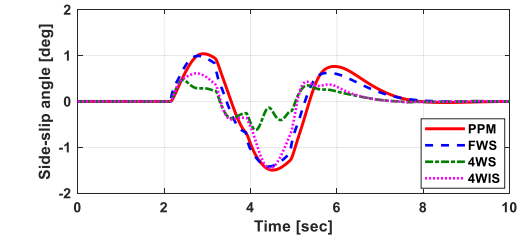

(d) Side-slip angles

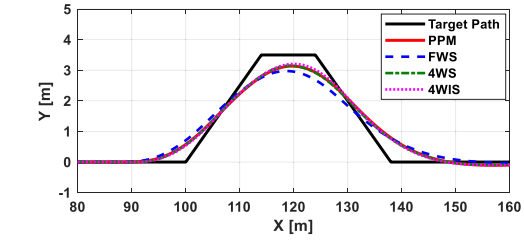

(e) Trajectories

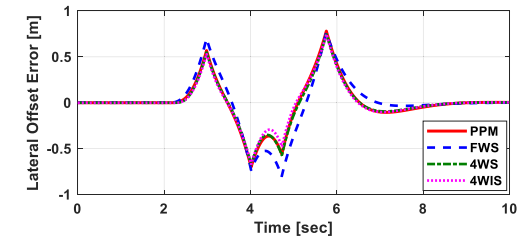

(f) Lateral offset errors

FIGURE 7. Simulation results for each controller with PATH-RYR.

Fig. 9 means that PPM-RYR and Method#1 are used for the reference yaw rate generation and the steering angle determination, respectively. As shown in Fig. 9-(a) and -(e), the steering wheel angles and lateral offset errors of PATH-RYR are smaller than those of PPM-RYR regardless of the methods of the steering angle determination. For the reason, PATH-RYR is preferred to PPM-RYR for the path tracking performance. On the other hand, as shown in Fig. 9-(d), the side-slip angle of 4WS with Method#2 is much smaller than those of 4WS with Method#1 or FWS and 4WIS with Method#2. Originally, 4WS has been known to be very effective for the reduction of the side-slip angle [17]–[19]. In this simulation, it is valid only for Method#2. On the contrary, 4WIS with Method#1 gives much larger side-slip angles, as shown in Fig. 9-(d). This means that it is not desirable to use 4WIS in terms of ride comfort. There are little differences among the reference yaw rates, the yaw rate errors and the lateral offset errors for each case [17]. In summary, it is recommended that PATH-RYR with 4WS and Method#2 is adopted for the path tracking control.

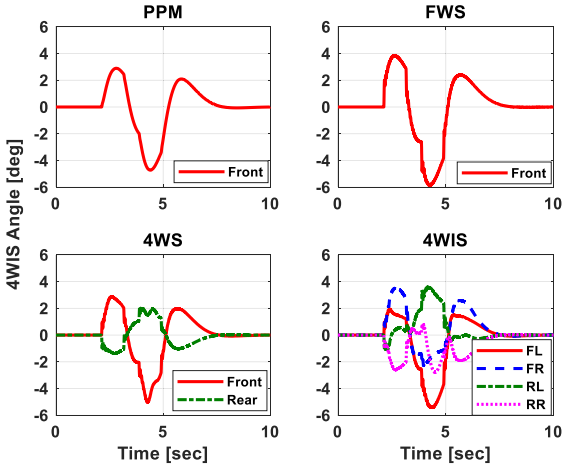

FIGURE 8. Steering angles of wheels for the pure pursuit method, FWS, 4WS and 4WIS with PPM-RYR.

B. EFFECTS OF ACTUATOR COMBINATIONS ON LOW FRICTION ROAD

Generally, 4WID and 4WIB have little effects on the yaw rate tracking performance [19] because 4WS and 4WIS are highly effective enough for path tracking control. However, the effects of 4WID and 4WIB on the path tracking performance have not been checked. To check the effects of 4WID and 4WIB, the second simulation was conducted with four actuator combinations, i.e., 4WIS, 4WIS+4WID, 4WIS+4WIB and 4WIS+4WIB+4WID, in the proposed path tracking controller. Let denote these actuator combinations as CASE1, CASE2, CASE3 and CASE4, respectively. PATH-RYR and Method#2 were used as the methods of the reference yaw rate generation and the steering angle determination, respectively. The simulation conditions were set to those given in the previous subsection except the vehicle speed and the tire-road friction coefficient were set to 50km/h and 0.6, respectively.

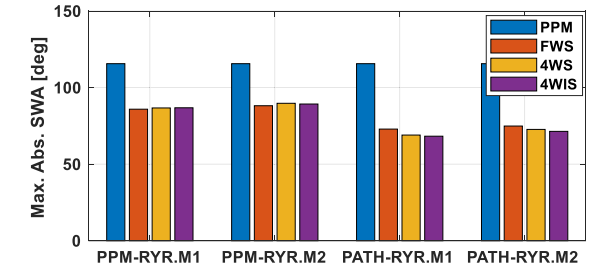

(a) Steering wheel angles

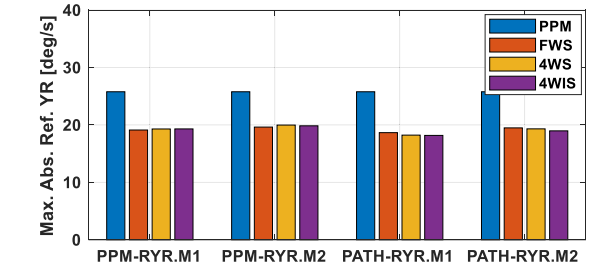

(b) Reference yaw rates

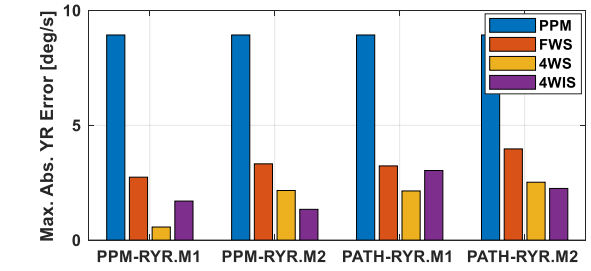

(c) Yaw rate errors

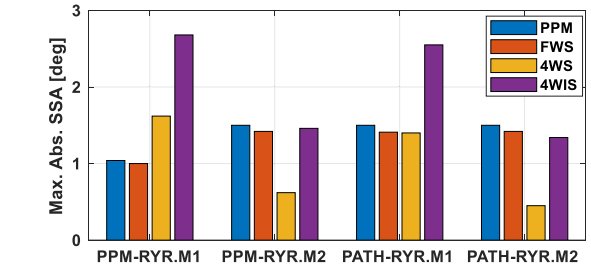

(d) Side-slip angles

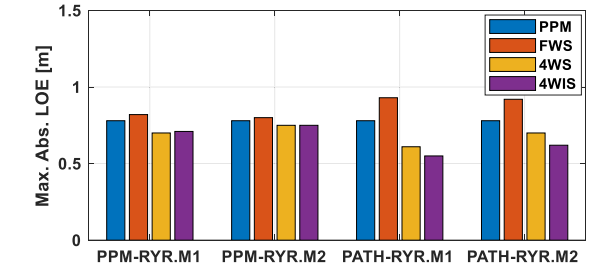

(e) Lateral offset errors

FIGURE 9. Maximum absolute values of each measure for each method and steering actuator.

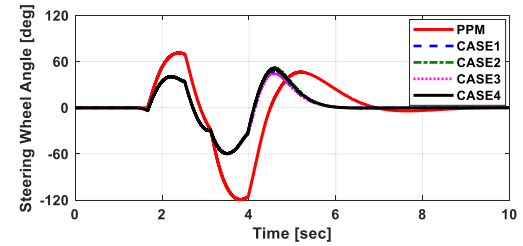

(a) Steering wheel angle of the pure pursuit method

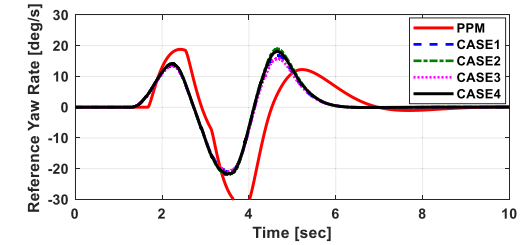

(b) Yaw rates from the pure pursuit method

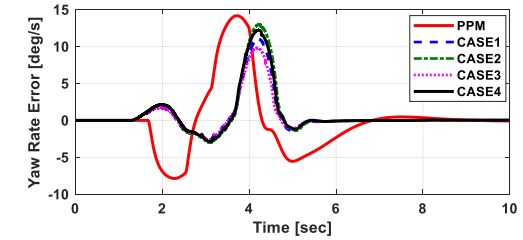

(c) Yaw rate erros

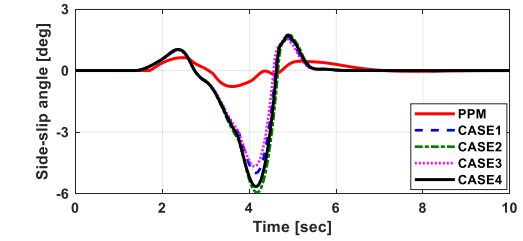

(d) Side-slip angles

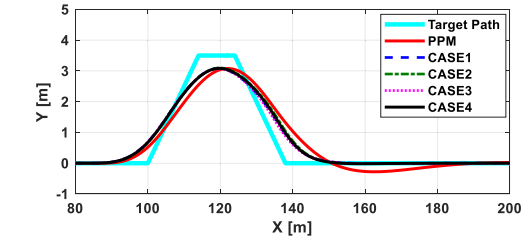

(e) Trajectories

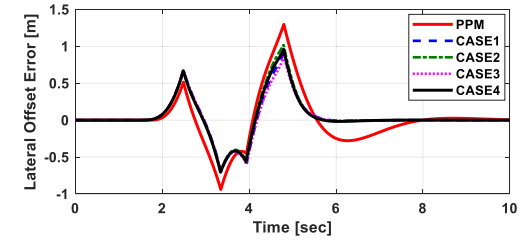

(f) Lateral offset errors

FIGURE 10. Simulation results for each controller with PPM-RYR.

Figs. 10 and 11 show the simulation results and the control inputs for each actuator combination. In the simulation results, the speed variation from the initial speed was less than 1km/h. So, it was not presented in the simulation results. As shown in Fig. 10, there are little differences among the actuator combinations in terms of the path tracking

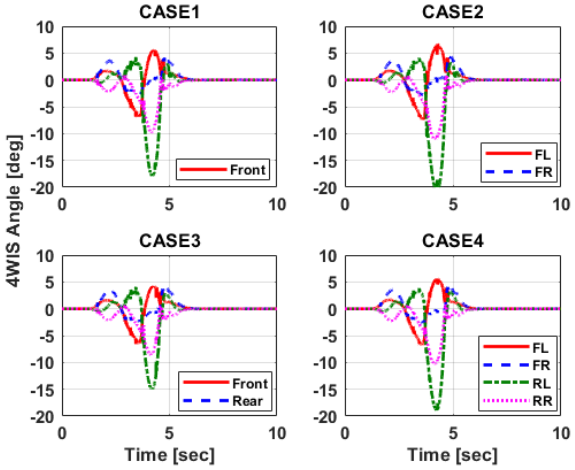

(a) Steering angles of each case

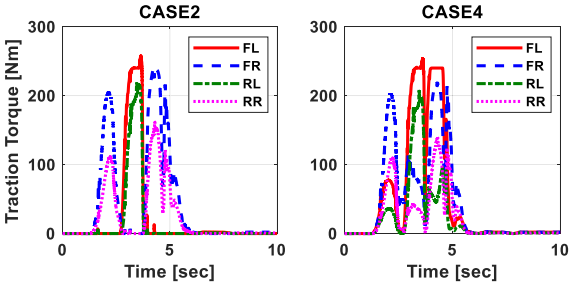

(b) Traction torques of 4WID of each case

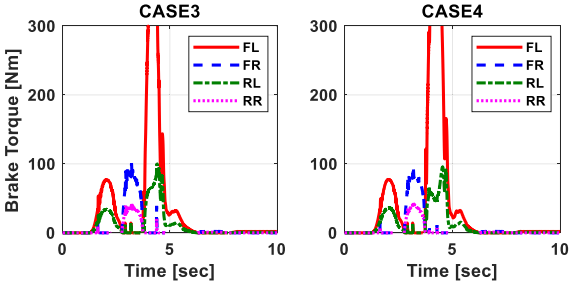

(c) Braking torques of 4WIB of each case

FIGURE 11. Steering angles of wheels for each case with PATH-RYR.

performance. Nevertheless, the path tracking performance of these actuator combinations is slightly better than of the pure pursuit method, as shown in Fig. 10-(e) and -(f). This is caused by the fact that the traction and braking torques of 4WID and 4WIB have an small effect on the control performance, as shown in Fig. 11. In general, the steering angles of active front steering (AFS) are reduced by the aid of 4WID, 4WIB and 4WID+4WIB [19]. However, the steering angles of 4WIS were not reduced with 4WID or 4WIB, as shown in Fig. 11-(a). This means that 4WIS itself is quite effective in generating the control yaw moment calculated from the upper-level controller. The identical results were given in the previous study [17]. For the reason, even though

TABLE 3. Average values of measures of 4WIS and 4WS for all cases.

Actuator	Measures	PPM-RYR.M1	PPM-RYR.M2	PATH-RYR.M1	PATH-RYR.M2
4WIS	SWA (deg)	69.0	70.1	69.0	69.8
	RefYR (deg/s)	20.9	21.5	20.9	21.4
	YRError (deg/s)	11.0	12.4	10.1	11.8
	SSA (deg)	6.4	7.0	6.1	6.7
	LOE (m)	1.265	1.250	1.198	1.288
4WS	SWA (deg)	69.6	72.1	69.4	71.6
	RefYR (deg/s)	21.0	22.0	20.1	21.8
	YRError (deg/s)	5.1	5.6	4.6	5.5
	SSA (deg)	3.0	2.8	2.8	2.9
	LOE (m)	0.935	0.940	0.910	0.935

the simulation is done under the identical conditions on high-friction roads, the identical conclusion can be drawn.

The simulation was done to check the effects of four actuator combinations, i.e., 4WIS, 4WIS+4WID, 4WIS+4WIB and 4WIS+4WIB+4WID, on low-friction roads. The simulation was done for the four cases corresponding to the combinations of PPM-RYR and PATH-RYR with Method#1 and Method#2.

Fig. 12 shows the maximum absolute values of each measure for four cases with 4WIS. The tick labels of x-axis in Fig. 12 are identical to those of Fig. 9. As shown in Fig. 12-(e), PATH-RYR with Method#2 shows the smaller lateral offset errors than the other combinations. On the other hand, as shown in Fig. 12-(d), the side-slip angles of all cases and combinations are quite large, compared to those of Fig. 9-(d). This means that the vehicle behaves under-steer, which is caused by the fact that the vehicle enters cornering on low-friction roads without speed reduction. The large side-slip angle can cause discomfort to passengers.

Fig. 13 shows the maximum absolute values of each measure for four cases with 4WS instead of 4WIS. Compared with Fig. 12-(d), the side-slip angles of Method#2 were significantly reduced with 4WS, as shown in Fig. 13-(d). This is the main effect of 4WS over the other actuators [19]. This means that 4WS is preferred to 4WIS in terms of ride comfort because large side-slip angle causes discomfort to passengers. As shown in Fig. 13-(e), the lateral offset errors of actuator combinations with 4WS gives nearly identical values to one another. Moreover, these values are smaller than those of 4WIS, as given in Fig. 12-(e). This means that there are little differences among the actuator combinations, 4WS, 4WS+4WID, 4WS+4WIB, 4WS+4WID+4WIB, in terms of the path tracking performance [17]. In summary, it is recommended to use 4WS instead of 4WIS without 4WID and 4WIB because 4WS is simple and cost-effective and can give better path tracking performance on low-friction roads.

Table 3 shows the average values of measures of 4WIS and 4WS for all cases, which were calculated from Figs 12 and 13. Table 4 shows the percentage reduction of

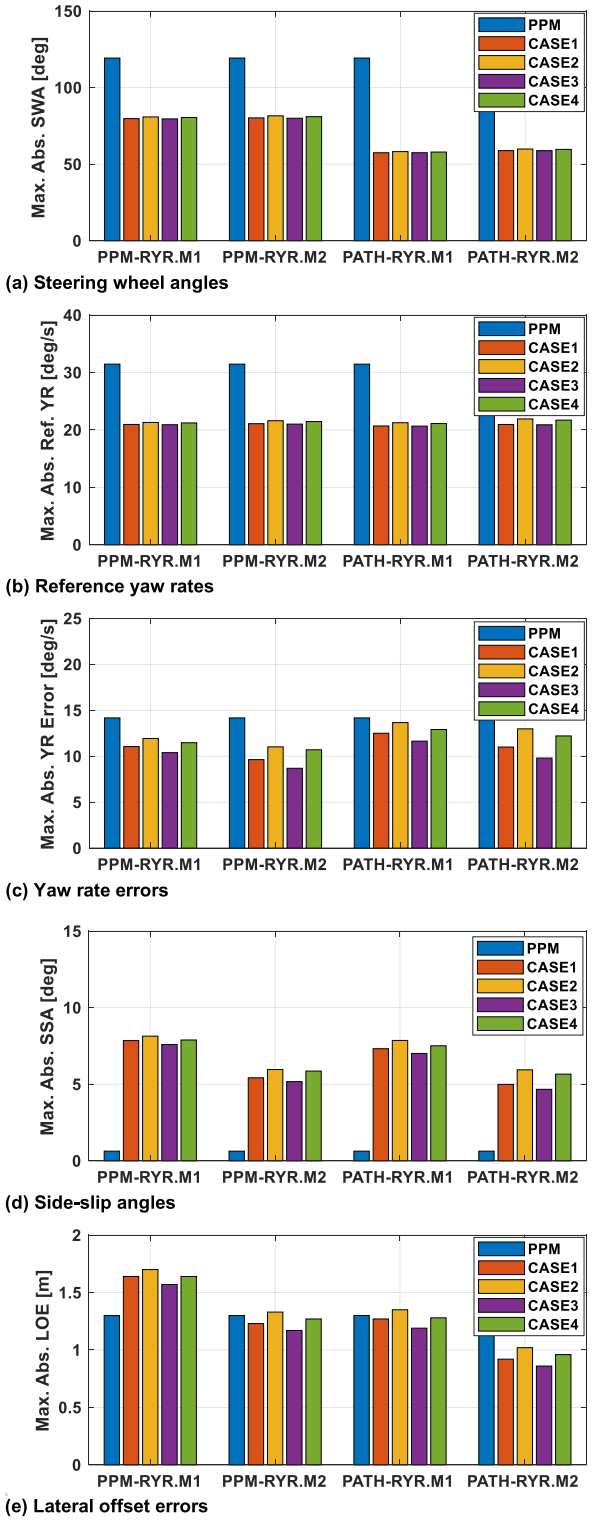

FIGURE 12. Maximum absolute values of each measure for actuator combinations with 4WIS.

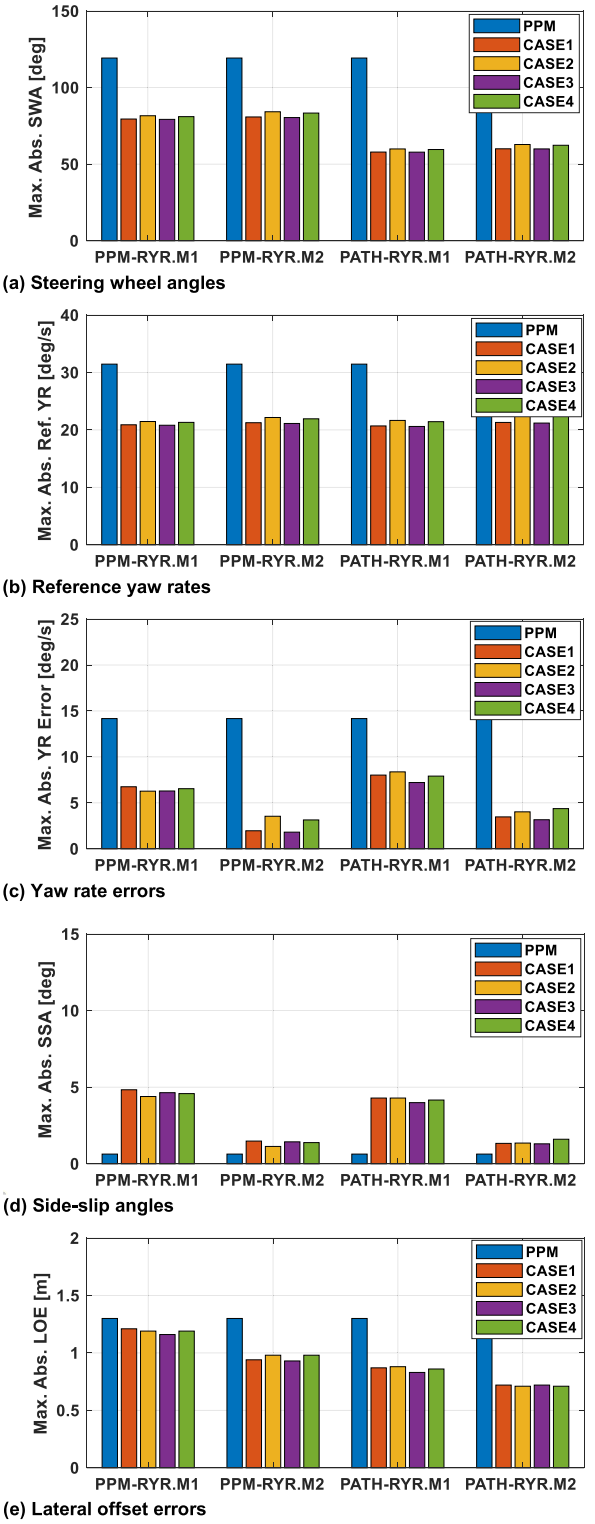

FIGURE 13. Maximum absolute values of each measure for actuator combinations with 4WS.

average values of 4WS with respect to 4WIS for all cases, which were calculated from Table 3. In these tables, SWA, RefYR, YRError, SSA and LOE represent the steering wheel angle, the reference yaw rate, the yaw rate error, the side-slip angle and the lateral offset error, respectively. As shown in Table 3, the steering wheel angles and the reference yaw rates of 4WS and 4WIS are nearly identical to each other. However, the yaw rate errors, the side-slip angles and the lateral offset

TABLE 4. Percentage reduction of average values of 4WS with respect to 4WIS for all cases.

Measures	PPM-RYR.M1	PPM-RYR.M2	PATH-RYR.M1	PATH-RYR.M2
SWA	-0.7	-2.9	-0.6	-2.6
RefYR	-0.6	-2.3	-0.3	-1.9
YRError	54.3	55.2	54.4	53.5
SSA	53.3	60.0	53.5	56.5
LOE	26.1	30.4	24.0	27.4

errors of 4WS are much smaller than those of 4WIS. This fact can be checked in Table 4. As shown in Table 4, the yaw rate errors and the side-slip angles of 4WS were reduced over 50% to those of 4WIS. The lateral offset error of 4WS were reduced over 25% to those of 4WIS. From these results, it can be concluded that 4WS is preferred to 4WIS in terms of the side-slip angle and the lateral offset error.

V. CONCLUSION

In this paper, the path tracking controller was designed for an in-wheel motor-driven electric vehicle with 4WIS, 4WID and 4WIB systems. The path tracking control problem is converted into the yaw rate tracking one. To derive the reference yaw rate, the pure pursuit and the path based methods were adopted. By using those methods, the drawbacks of the error dynamics based method can be avoided. For yaw rate tracking control, a direct yaw moment control was adopted to calculate the control yaw moment. To distribute the control yaw moment into tire forces generated by 4WIS, 4WID and 4WIB, the control allocation method, WPCA, was adopted. In WPCA, several actuator combinations were represented by corresponding vectors of virtual weights in the objective function of WPCA. The proposed method was implemented on MATLAB/Simulink and CarSim. Simulation was conducted to verify the performance of the proposed method. From the simulation results, it was shown that the proposed method is effective when improving the path tracking performance, and that 4WID and 4WIB have little effects on the control performance of 4WS or 4WIS regardless of tire-road friction. Moreover, it was also shown from the simulation results that 4WS is preferred to 4WIS regardless of tire-road friction and any actuator combinations in terms of ride comfort because it can control the vehicle with 50% smaller side-slip angle and 25% smaller lateral offset error than 4WIS. Hence, it can be concluded that 4WS itself is quite effective for path tracking control and ride comfort. The drawback of the proposed method is that it cannot be applied when the vehicle speed is very low. Therefore, further research will include a path tracking control with 4WS or 4WIS at low speeds below 3m/s.

REFERENCES

[1] E. Yurtsever, J. Lambert, A. Carballo, and K. Takeda, "A survey of autonomous driving: Common practices and emerging technologies," *IEEE Access*, vol. 8, pp. 58443–58469, 2020, doi: 10.1109/ACCESS.2020.2983149.

[2] C. Badue, R. Guidolini, R. V. Carneiro, P. Azevedo, V. B. Cardoso, A. Forechi, L. Jesus, R. Berriel, T. M. Paixao, F. Mutz, and L. De P. Veronese, "Self-driving cars: A survey," *Exp. Syst. Appl.*, vol. 165, Mar. 2021, Art. no. 113816, doi: 10.1016/j.eswa.2020.113816.

[3] A. S. Aguiar, F. N. dos Santos, J. B. Cunha, H. Sobreira, and A. J. Sousa, "Localization and mapping for robots in agriculture and forestry: A survey," *Robotics*, vol. 9, no. 4, p. 97, Nov. 2020, doi: 10.3390/robotics9040097.

[4] T. A. Johansen and T. I. Fossen, "Control allocation—A survey," *Automatica*, vol. 49, no. 5, pp. 1087–1103, Mar. 2013, doi: 10.1016/j.automatica.2013.01.035.

[5] T. Hiraoka, O. Nishihara, and H. Kumamoto, "Automatic path-tracking controller of a four-wheel steering vehicle," *Vehicle Syst. Dyn.*, vol. 47, no. 10, pp. 1205–1227, Oct. 2009, doi: 10.1080/00423110802545919.

[6] J. Wang, R. Wang, H. Jing, and N. Chen, "Coordinated active steering and four-wheel independently driving/braking control with control allocation," *Asian J. Control*, vol. 18, no. 1, pp. 98–111, Jan. 2016, doi: 10.1002/asjc.1235.

[7] R. Potluri and A. K. Singh, "Path-tracking control of an autonomous 4WS4WD electric vehicle using its natural feedback loops," *IEEE Trans. Control Syst. Technol.*, vol. 23, no. 5, pp. 2053–2062, Sep. 2015, doi: 10.1109/TCST.2015.2395994.

[8] C. Hu, R. Wang, and F. Yan, "Integral sliding mode-based composite nonlinear feedback control for path following of four-wheel independently actuated autonomous vehicles," *IEEE Trans. Transport. Electrific.*, vol. 2, no. 2, pp. 221–230, Jun. 2016, doi: 10.1109/TTE.2016.2537046.

[9] P. Hang, X. Chen, and F. Luo, "LPV/H_∞ controller design for path tracking of autonomous ground vehicles through four-wheel steering and direct yaw-moment control," *Int. J. Automot. Technol.*, vol. 20, no. 4, pp. 679–691, Aug. 2019, doi: 10.1007/s12239-019-0064-1.

[10] X. Chen, Y. Peng, P. Hang, and T. Tang, "Path tracking control of four-wheel independent steering electric vehicles based on optimal control," in *Proc. 39th Chin. Control Conf. (CCC)*, Shenyang, China, Jul. 2020, pp. 5436–5442, doi: 10.23919/CCC50068.2020.9189047.

[11] Y. Liang, Y. Li, L. Zheng, Y. Yu, and Y. Ren, "Yaw rate tracking-based path-following control for four-wheel independent driving and four-wheel independent steering autonomous vehicles considering the coordination with dynamics stability," *Proc. Inst. Mech. Eng. D, J. Automobile Eng.*, vol. 235, no. 1, pp. 260–272, Jan. 2021, doi: 10.1177/0954407020938490.

[12] Y. Jeong and S. Yim, "Model predictive control-based integrated path tracking and velocity control for autonomous vehicle with four-wheel independent steering and driving," *Electronics*, vol. 10, no. 22, p. 2812, Nov. 2021, doi: 10.3390/electronics10222812.

[13] L. Zhai, T. Sun, and J. Wang, "Electronic stability control based on motor driving and braking torque distribution for a four in-wheel motor drive electric vehicle," *IEEE Trans. Veh. Technol.*, vol. 65, no. 6, pp. 4726–4739, Jun. 2016, doi: 10.1109/TVT.2016.2526663.

[14] L. Jin, L. Gao, Y. Jiang, M. Chen, Y. Zheng, and K. Li, "Research on the control and coordination of four-wheel independent driving/steering electric vehicle," *Adv. Mech. Eng.*, vol. 9, no. 4, pp. 1–13, 2017, doi: 10.1177/1687814017698877.

[15] P. Hang, X. Chen, and F. Luo, "Path-tracking controller design for a 4WIS and 4WID electric vehicle with steer-by-wire system," SAE Tech. Paper 2017-01-1954, 2017, doi: 10.4271/2017-01-1954.

[16] P. Hang and X. Chen, "Integrated chassis control algorithm design for path tracking based on four-wheel steering and direct yaw-moment control," *Proc. Inst. Mech. Eng., I, J. Syst. Control Eng.*, vol. 233, no. 6, pp. 625–641, Jul. 2019, doi: 10.1177/0959651818806075.

[17] J. Nah and S. Yim, "Vehicle stability control with four-wheel independent braking, drive and steering on in-wheel motor-driven electric vehicles," *Electronics*, vol. 9, no. 11, p. 1934, Nov. 2020, doi: 10.3390/electronics9111934.

[18] S. Yim, "Comparison among active front, front independent, 4-wheel and 4-wheel independent steering systems for vehicle stability control," *Electronics*, vol. 9, no. 5, p.798, 2020, doi: 10.3390/electronics9050798.

[19] S. Yim, "Coordinated control with electronic stability control and active steering devices," *J. Mech. Sci. Technol.*, vol. 29, no. 12, pp. 5409–5416, 2015, doi: 10.1007/s12206-015-1142-6.

[20] J. Nah and S. Yim, "Optimization of control allocation with ESC, AFS, ARS and TVD in integrated chassis control," *J. Mech. Sci. Technol.*, vol. 33, no. 6, pp. 2941–2948, Jun. 2019, doi: 10.1007/s12206-019-0541-5.

[21] Y. Furukawa, N. Yuhara, S. Sano, H. Takeda, and Y. Matsushita, "A review of four-wheel steering studies from the viewpoint of vehicle dynamics and control," *Vehicle Syst. Dyn.*, vol. 18, nos. 1–3, pp. 151–186, Jan. 1989, doi: 10.1080/00423118908968917.
[22] A. T. van Zanten, R. Erhardt, and G. Pfaff, "VDC, the vehicle dynamics control system of Bosch," SAE Tech. Paper 950759, 1995, doi: 10.4271/950759.
[23] P. Koehn and M. Eckrich, "Active steering—The BMW approach towards modern steering technology," SAE Tech. Paper 2004-01-1105, 2004, doi: 10.4271/2004-01-1105.
[24] M. Croft-White and M. Harrison, "Study of torque vectoring for all-wheel-drive vehicles," *Vehicle Syst. Dyn.*, vol. 44, pp. 313–320, Jan. 2006, doi: 10.1080/00423110600871400.
[25] M. Jonasson, S. Zetterström, and A. S. Trigell, "Autonomous corner modules as an enabler for new vehicle chassis solutions," in *Proc. FISITA World Automot. Congr.*, 2006, p. F2006V054T. [Online]. Available: http://urn.kb.se/resolve?urn=urn:nbn:se:kth:diva-6769 and https://go.fisita.com/store/bookstore/fisita-transactions-2006-ihY09aNE
[26] W. Wang and X. Chen, "Design methodology for wheel corner module topology based on position and orientation characteristics," *Mechanism Mach. Theory*, vol. 136, pp. 122–140, Jun. 2019, doi: 10.1016/j.mechmachtheory.2019.02.017.
[27] B. Paden, M. Čáp, S. Z. Yong, D. Yershov, and E. Frazzoli, "A survey of motion planning and control techniques for self-driving urban vehicles," *IEEE Trans. Intell. Vehicles*, vol. 1, no. 1, pp. 33–55, Jun. 2016, doi: 10.1109/TIV.2016.2578706.
[28] A. Sorniotti, P. Barber, and S. De Pinto, "Path tracking for automated driving: A tutorial on control system formulations and ongoing research," in *Automated Driving*, D. Watzenig and M. Horn, Eds. Cham, Switzerland: Springer, 2017, doi: 10.1007/978-3-319-31895-0_5.
[29] N. H. Amer, H. Zamzuri, K. Hudha, and Z. A. Kadir, "Modelling and control strategies in path tracking control for autonomous ground vehicles: A review of state of the art and challenges," *J. Intell. Robot. Syst.*, vol. 86, no. 2, pp. 225–254, May 2017, doi: 10.1007/s10846-016-0442-0.
[30] G. Bai, Y. Meng, L. Liu, W. Luo, Q. Gu, and L. Liu, "Review and comparison of path tracking based on model predictive control," *Electronics*, vol. 8, no. 10, p. 1077, Sep. 2019, doi: 10.3390/electronics8101077.
[31] Q. Yao, Y. Tian, Q. Wang, and S. Wang, "Control strategies on path tracking for autonomous vehicle: State of the art and future challenges," *IEEE Access*, vol. 8, pp. 161211–161222, 2020, doi: 10.1109/ACCESS.2020.3020075.
[32] M. Rokonuzzaman, N. Mohajer, S. Nahavandi, and S. Mohamed, "Review and performance evaluation of path tracking controllers of autonomous vehicles," *IET Intell. Transp. Syst.*, vol. 15, no. 5, pp. 646–670, May 2021, doi: 10.1049/itr2.12051.
[33] P. Raksincharoensak, M. Nagai, and H. Mouri, "Investigation of automatic path tracking control using four-wheel steering vehicle," in *Proc. IEEE Int. Vehicle Electron. Conf. (IVEC)*, Tottori, Japan, Sep. 2001, pp. 73–77, doi: 10.1109/IVEC.2001.961729.
[34] R. Wang, G. Yin, J. Zhuang, N. Zhang, and J. Chen, "The path tracking of four-wheel steering autonomous vehicles via sliding mode control," in *Proc. IEEE Vehicle Power Propuls. Conf. (VPPC)*, Hangzhou, China, Oct. 2016, pp. 17–20, doi: 10.1109/VPPC.2016.7791799.
[35] R. Wang, G. Yin, and X. Jin, "Robust adaptive sliding mode control for nonlinear four-wheel steering autonomous vehicles path tracking systems," in *Proc. IEEE 8th Int. Power Electron. Motion Control Conf. (IPEMC-ECCE Asia)*, Hefei, China, May 2016, pp. 2999–3006, doi: 10.1109/IPEMC.2016.7512774.
[36] M. Deremetz, R. Lenain, A. Couvent, C. Cariou, and B. Thuilot, "Path tracking of a four-wheel steering mobile robot: A robust off-road parallel steering strategy," in *Proc. Eur. Conf. Mobile Robots (ECMR)*, Paris, France, Sep. 2017, pp. 6–8, doi: 10.1109/ECMR.2017.8098670.
[37] P. Hang, F. Luo, S. Fang, and X. Chen, "Path tracking control of a four-wheel-independent-steering electric vehicle based on model predictive control," in *Proc. 36th Chin. Control Conf. (CCC)*, Dalian, China, Jul. 2017, pp. 26–28, doi: 10.23919/ChiCC.2017.8028849.
[38] Q. Tan, P. Dai, Z. Zhang, and J. Katupitiya, "MPC and PSO based control methodology for path tracking of 4WS4WD vehicles," *Appl. Sci.*, vol. 8, no. 6, p. 1000, Jun. 2018, doi: 10.3390/app8061000.
[39] Q. Du, C. Zhu, Q. Li, B. Tian, and L. Li, "Optimal path tracking control for intelligent four-wheel steering vehicles based on MPC and state estimation," *Proc. Inst. Mech. Eng., D, J. Automobile Eng.*, vol. 236, no. 9, pp. 1964–1976, Aug. 2022, doi: 10.1177/09544070211054318.
[40] X. Tan, D. Liu, and H. Xiong, "Optimal control method of path tracking for four-wheel steering vehicles," *Actuators*, vol. 11, no. 2, p. 61, Feb. 2022, doi: 10.3390/act11020061.
[41] Y. Liang, Y. Li, Y. Yu, and L. Zheng, "Integrated lateral control for 4WID/4WIS vehicle in high-speed condition considering the magnitude of steering," *Vehicle Syst. Dyn.*, vol. 58, no. 11, pp. 1711–1735, Nov. 2020, doi: 10.1080/00423114.2019.1645343.
[42] E. Katsuyama, M. Yamakado, and M. Abe, "A state-of-the-art review: Toward a novel vehicle dynamics control concept taking the driveline of electric vehicles into account as promising control actuators," *Vehicle Syst. Dyn.*, vol. 59, no. 7, pp. 976–1025, Jul. 2021, doi: 10.1080/00423114.2021.1916048.
[43] H. Y. Wong, "Handling chateristics of road vehicles," in *Theory of Ground Vehicles*, 3rd ed. NewYork, NY, USA: Wiley, 2001, ch. 5, sec. 6, p. 361.
[44] R. Rajamani, "Lateral vehicle dynamics," in *Vehicle Dynamics and Control*, 1st ed. NewYork, NY, USA: Springer, 2005, ch. 2, sec. 6, p. 40.
[45] H. H. Kim and J. Ryu, "Sideslip angle estimation considering short-duration longitudinal velocity variation," *Int. J. Automot. Technol.*, vol. 12, no. 4, pp. 545–553, Aug. 2011, doi: 10.1007/s12239-011-0064-2.
[46] G. Baffet, A. Charara, and D. Lechner, "Estimation of vehicle sideslip, tire force and wheel cornering stiffness," *Control Eng. Pract.*, vol. 17, no. 11, pp. 1255–1264, Nov. 2009, doi: 10.1016/j.conengprac.2009.05.005.
[47] J. Wang, J. M. Solis, and R. G. Longoria, "On the control allocation for coordinated ground vehicle dynamics control systems," in *Proc. Amer. Control Conf.*, New York, NY, USA, Jul. 2007, pp. 5724–5729, doi: 10.1109/ACC.2007.4282308.
[48] S. Yim, J. Choi, and K. Yi, "Coordinated control of hybrid 4WD vehicles for enhanced maneuverability and lateral stability," *IEEE Trans. Veh. Technol.*, vol. 61, no. 4, pp. 1946–1950, May 2012, doi: 10.1109/TVT.2012.2188921.
[49] L. Pinto, S. Aldworth, M. Watkinson, P. Jeary, and M. Franco-Jorge, "Advanced yaw motion control of a hybrid vehicle using twin rear electric motors," in *Proc. 10th Int. Symp. Adv. Vehicle Control*, Loughborough, U.K., 2010, pp. 640–645.
[50] *VS Browser: Reference Manual, The Graphical User Interfaces of BikeSim, CarSim, and TruckSim*, Mechanical Simulation Corporation, Ann Arbor, MI, USA, 2009.

YONGHWAN JEONG received the B.S. and Ph.D. degrees in mechanical engineering from Seoul National University, South Korea, in 2014 and 2020, respectively. From 2020 to 2021, he was a Senior Research Engineer with Hyundai Motor Company, South Korea. Since 2021, he has been an Assistant Professor with the Department of Mechanical and Automotive Engineering, Seoul National University of Science and Technology, South Korea. His research interests include sensor fusion with vehicular communication, risk assessment, driver intention inference with trajectory prediction, motion planning, and control of urban automated vehicle.

SEONGJIN YIM (Member, IEEE) received the B.S. degree in mechanical engineering from Yonsei University, South Korea, in 1995, and the M.S. and Ph.D. degrees in mechanical engineering from the Korea Advanced Institute of Science and Technology (KAIST), in 1997 and 2007, respectively.

From 2008 to 2010, he was a Postdoctoral Researcher with the BK21 School for Creative Engineering Design of Next Generation Mechanical and Aerospace Systems, Seoul National University. From 2011 to 2013, he was a Research Professor with the Advanced Institutes of Convergence Technology, Seoul National University. Since 2019, he has been an Associate Professor with the Department of Mechanical and Automotive Engineering, Seoul National University of Science and Technology, South Korea. His research interests include integrated chassis control systems with V2V communication, cloud computing-based vehicle control, electric power steering, and steer-by-wire systems.